



HAL
open science

Application of the Mise-à-la-Masse method to detect the bottom leakage of water reservoirs

C. Ling, A. Revil, Y. Qi, F. Abdulsamad, P. Shi, Sylvie Nicaise, Laurent Peyras

► To cite this version:

C. Ling, A. Revil, Y. Qi, F. Abdulsamad, P. Shi, et al.. Application of the Mise-à-la-Masse method to detect the bottom leakage of water reservoirs. *Engineering Geology*, 2019, 261, pp.105272. 10.1016/j.enggeo.2019.105272 . hal-02324231

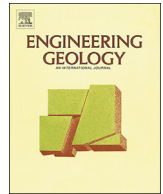
HAL Id: hal-02324231

<https://hal.science/hal-02324231>

Submitted on 23 Nov 2020

HAL is a multi-disciplinary open access archive for the deposit and dissemination of scientific research documents, whether they are published or not. The documents may come from teaching and research institutions in France or abroad, or from public or private research centers.

L'archive ouverte pluridisciplinaire **HAL**, est destinée au dépôt et à la diffusion de documents scientifiques de niveau recherche, publiés ou non, émanant des établissements d'enseignement et de recherche français ou étrangers, des laboratoires publics ou privés.



Application of the Mise-à-la-Masse method to detect the bottom leakage of water reservoirs

C. Ling^{a,b}, A. Revil^{b,*}, Y. Qi^b, F. Abdulsamad^b, P. Shi^c, S. Nicaise^d, L. Peyras^d

^a State Key Laboratory of Geohazard Prevention and Geoenvironment Protection, Chengdu University of Technology, 1#, Dongsanlu, Erxianqiao, Chengdu 610059, Sichuan, PR China

^b Univ. Grenoble Alpes, Univ. Savoie Mont Blanc, CNRS, IRD, IFSTTAR, ISTERRE, 38000 Grenoble, France

^c Department of Mechanics, Harbin Institute of Technology, Harbin, People's Republic of China

^d IRSTEA, Aix-en-Provence, France

ARTICLE INFO

Keywords:

Mise-à-la-Masse
Bottom leakage
Water reservoir
Tikhonov regularization

ABSTRACT

Leakages of reservoirs are responsible for the loss of water resources and the spread of contaminants. We develop a methodology to detect leaks located at the bottom side of a reservoir with the minimally invasive mise-à-la-masse method, which involves the potential electrodes located at the ground surface around the reservoir and the current source and sink placed in and out of the reservoir, respectively. This method allows localizing the secondary current distribution associated with leakage using the distribution of potential recorded on a set of electrodes during the mise-à-la-masse experiment. An initial model based on the distribution of root mean square values between the observation and the simulation data is first given to the inversion algorithm. The Tikhonov regularization, which includes a weighting matrix and a minimum support function, is used to strengthen the detection resolution of the leak. 29 sandbox experiments show that the proposed method and inversion algorithm can localize a single leak. For a leak with a crack shape, the inversion algorithm detects the location of the leak with a small bias. When the leak lasts, a conductive zone may occur below the leak due to the increase of water content or ionic strength of the pore water. The occurrence of such a conductive body could affect the localization of the leak because the conductivity distribution may not be well-resolved. The effect is analyzed using synthetic experiments. The results show that the bias between the real leak and inversion results increases with the position and size of the undetected conductive zone. Two small-scale field tests were conducted to test the performance of the mise-à-la-masse method. The two leaks are properly identified. This study provides an efficient approach to detect the bottom leakage of reservoirs.

1. Introduction

Water reservoirs are used for agricultural and industrial purposes (e.g., [Votruba and Broža, 1989](#)). Leakage causes the losses of precious water resources. They may also affect the stability and integrity of the infrastructures (e.g., [Poulain et al., 2011](#); [Lee et al., 2005](#)). In addition, synthetic geomembranes are widely used in the chemical or mining industries. An unexpected leak in such reservoirs can cause serious contamination to the surrounding soils and groundwater environments ([Mostafa et al., 2016](#)). Hence, the early identification of leakage is very important for the safe operation of these reservoirs ([Peyras et al., 2008](#)).

Several non-geophysical methods have been developed in civil engineering to detect leaks of reservoirs or ponds. The most common methods are volumetric and mass balancing measurements, statistical

inventory reconciliation, liquid sensing probes, and distributed fiber optic sensor (see [Colombo et al., 2009](#), for a review). In the volumetric and mass balancing measurements and the statistical inventory reconciliation, an unexplained loss of mass is used to indicate the presence of a leak, but the positions of leaks cannot be resolved ([Musthafa et al., 2017](#)). Liquid sensing probes (e.g., time-domain reflectometer, piezometer, and conductivity meter) can be buried at specific locations and then used to monitor the variations in water content, pressure, and salinity over time ([O'Connor and Dowding, 1999](#)). The distributed fiber optic sensor can perceive the temperature variations and be used to detect leaks as well. The signal from fiber optic sensor can be determined by using the optoelectronic instruments. ([Selker et al., 2006](#)). The fiber optic buried at strategic locations inside the dam or dike can intercept the temperature changes due to the leakage ([Khan et al.,](#)

* Corresponding author.

E-mail addresses: lingcp2015@163.com (C. Ling), andre.revil@univ-smb.fr (A. Revil), feras.abdul-samad@univ-smb.fr (F. Abdulsamad), 16B318003@hit.edu.cn (P. Shi), sylvie.nicaise@irstea.fr (S. Nicaise), laurent.peyras@irstea.fr (L. Peyras).

<https://doi.org/10.1016/j.enggeo.2019.105272>

Received 13 June 2019; Received in revised form 27 August 2019; Accepted 27 August 2019

Available online 28 August 2019

0013-7952/ © 2019 Elsevier B.V. All rights reserved.

2010). However, if a suspected leakage took place during the operation of a water reservoir and no sensor was pre-embedded in the vicinity of the leak, it is notoriously difficult to localize the leak.

Due to the minimally invasive and efficient measurements, several geophysical methods (i.e., electrical resistivity tomography, self-potential method, *mise-à-la-masse*) can be used to detect leakages. As an active technique, electrical resistivity tomography can image the temporal and spatial resistivity distribution (Daily et al., 2004). Resistivity anomalies can be used under restrictive conditions to detect flow paths in dams and embankments (Ramirez et al., 1996; Francisco José et al., 2018; Himi et al., 2018; Abdulsamad et al., 2019). The self-potential method is a passive geophysical method to measure the natural electrical potential associated with ground water flow through electrokinetic coupling (Revil and Jardani, 2013). When there is a leakage in the dam or dike, the significant electrical potential anomalies associated with the flow of pore water can be indeed detected (Panthulu et al., 2001; Rozycki, 2009; Soueid Ahmed et al., 2019).

The *mise-à-la-masse* method is a simple and yet powerful geophysical technique to detect leaks especially in reservoirs with an insulating geomembrane. The underlying idea is to inject the electrical current in a water (conductive) body. The current would preferentially flow through the leak. The resulting electrical potential distribution can be measured on the ground surface. In practice, a pair of current electrodes are used and a number of voltage measurements relative to a remote reference point are carried out. The electrical current injected in the conductive body with the positive current electrode (A) flows to the negative current electrode (B) placed relatively far from the conductive body to form a bipole. By using a mobile potential electrode (M), the electrical potential with respect to the remote reference potential electrode (N) can be logged. The contour map of electrical potential provides useful information with regard to the shape of the conductive body. The *mise-à-la-masse* method has been used to map the ore mineral (Ketola, 1972), to find out the flow direction of groundwater (Pant, 2004; Perri et al., 2018), to delineate conductive tracer plumes (De Carlo et al., 2013), and to evaluate the leakage of reservoir (Binley et al., 1997; Ling et al., 2019).

Ling et al. (2019) recently proposed a method similar to what was initially developed for the inversion of self-potential data (Haas et al., 2013) to invert the voltages recorded by the *mise-à-la-masse* method. A depth-weighting matrix and a minimum support function are used in the inversion algorithm to identify the precise locations of leakages. The validation of the inversion method was tested by some experiments about leaks on the side faces of a reservoir in the laboratory. Compared to the side leak, the bottom leak in the reservoir, which is a common situation, is more difficult to be detected due to the weaker electrical signals during a *mise-à-la-masse* experiment.

The goal of the present study is to advance the *mise-à-la-masse* method and corresponding inversion algorithm for detecting the bottom leakage of the water reservoir with impervious and insulating geomembranes. In this study, 29 sandbox experiments are carried out. We also improve the inversion method to get better results, and discuss the effect of an undetected conductive zone due to the leakage on the inversion results. In addition, the *mise-à-la-masse* method was verified by two small-scale field tests and synthetic experiments.

2. Materials and methods

2.1. Laboratory experiment setup

To evaluate the bottom leakage detection of a water reservoir with the *mise-à-la-masse* method, a plexiglass sandbox was used. Its dimensions are 53.7 cm by 28.5 cm by 33.4 cm, (see Fig. 1). In the laboratory experiments, the sandbox was filled with the silica sand, the chemical composition of which is SiO₂ (98%), Al₂O₃ (0.9%), K₂O (0.5%), and others (0.6%). The dry density and porosity of this sand are 1.4 g/cm³ and 0.37 ± 0.01, respectively. The total thickness of the

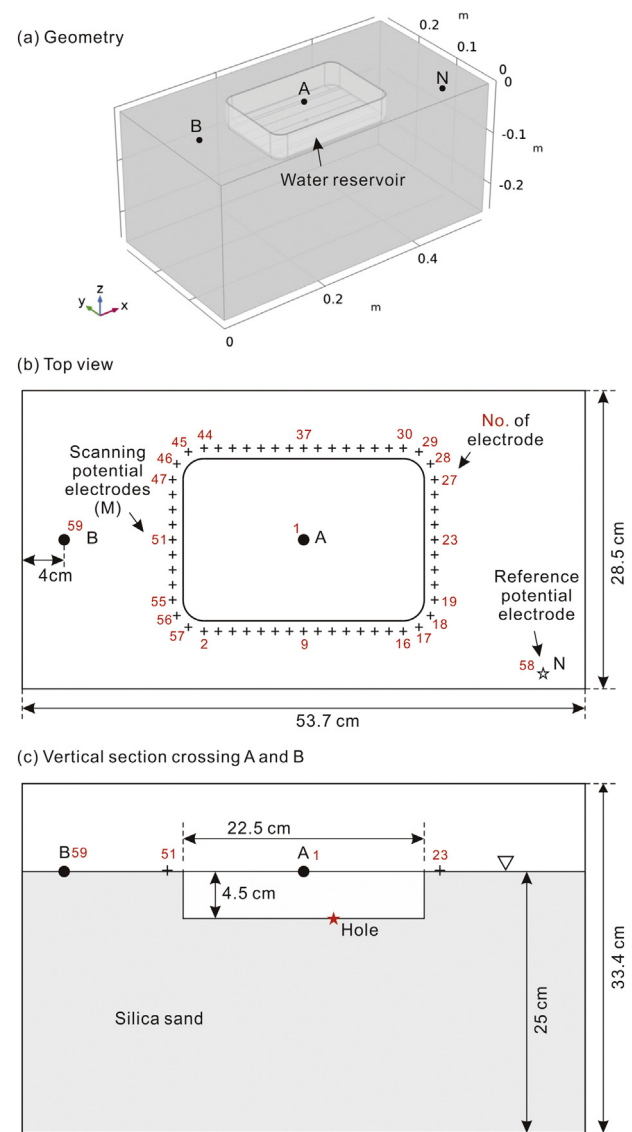


Fig. 1. Sketch of the sandbox with the plastic container used to simulate a leaking reservoir. The positive current electrode A (red label 1) is placed inside the reservoir, while the negative current electrode B (red label 59) is located 11.6 cm from the reservoir. The 56 scanning electrodes M labeled by their number (see the red labels 2–57) are arranged around the reservoir. The voltage electrode N (i.e., the red label 58) is located at a distance of 12 cm from the reservoir. This electrode is used as a reference for measuring the electrical potential distributions. This geometry is used for the physical and synthetic (numerical) experiments. (For interpretation of the references to colour in this figure legend, the reader is referred to the web version of this article.)

silica sand in the sandbox was 25 cm.

Tap water with an electrical conductivity of $\sim 900 \mu\text{S}/\text{cm}$ (25 °C) was used to saturate the silica sand. The electrical resistivity of the water-saturated sand is $\sim 50 \Omega\text{m}$ at room temperature (20 °C). During the sand packing processes, water was first added, and then the sand grains were packed layer by layer until the prescribed thickness of sand was reached, in order to minimize the entrapment of gas bubbles. The sand was settled by gravity for more than 24 h, and the excess water above the sandbox surface was removed prior performing the *mise-à-la-masse* experiments.

A plastic cubic reservoir with the dimensions of 22.5 cm length, 15.0 cm width, and 4.7 cm height was used to simulate the water reservoir. The water reservoir was placed in the top center of the sand. The top of the reservoir is flush with the sand surface (Fig. 1). The water

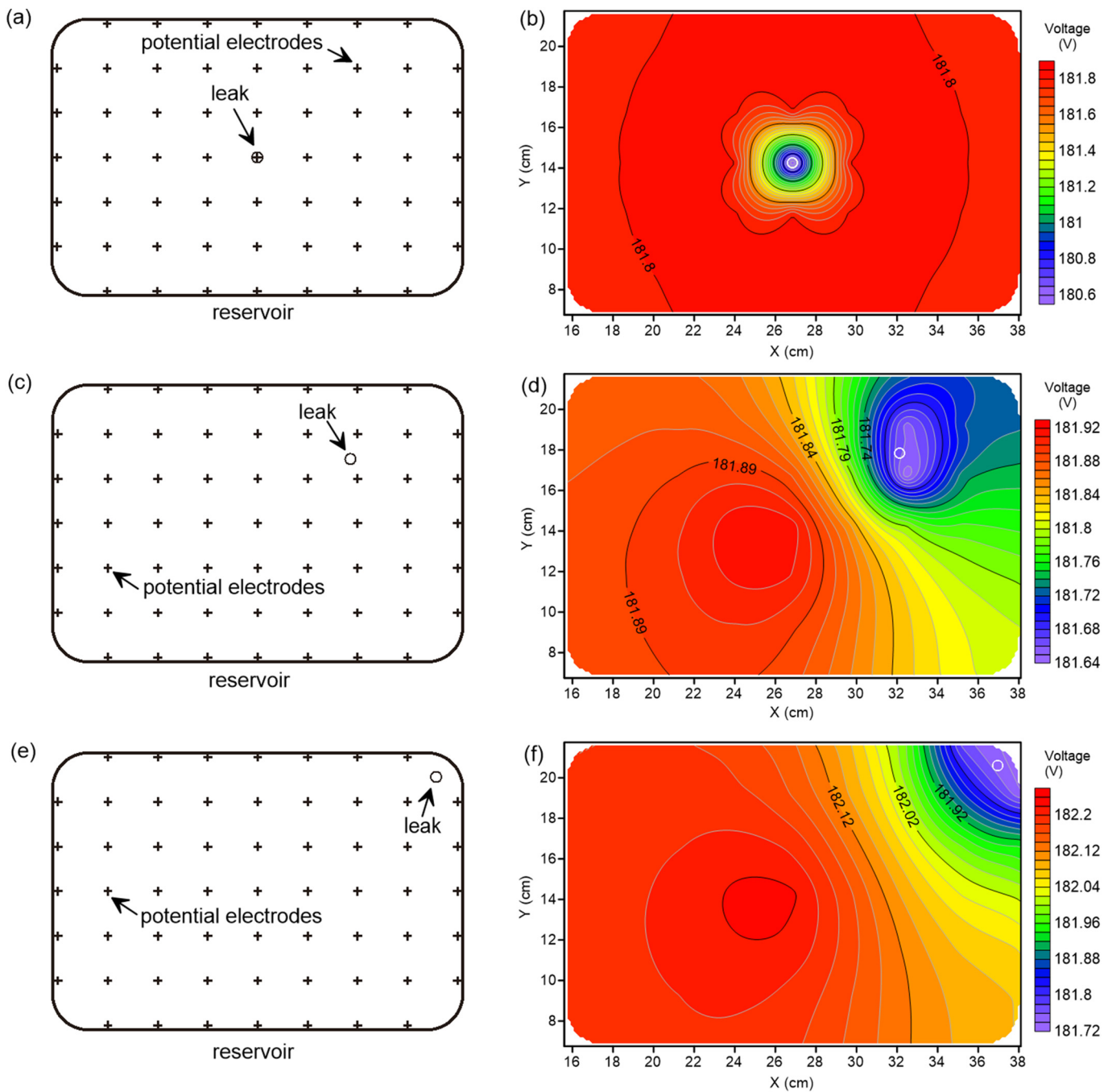


Fig. 2. Locations of the leak (left) and the corresponding contour maps (right) of electrical potentials (synthetic experiments). The scanning potential electrodes (i.e., the cross in the figure) are equidistantly located at the bottom of the reservoir. There are a total of 59 potential electrodes used to sample the electrical potential distribution. In the contour maps (right), the white open circles denote the locations of the leak. The minimum voltages are close to the locations of leaks. (a, b). Geometry and voltage distribution for a leak centered in the center of the bottom part of the reservoir. (c, d). Geometry and voltage distribution for a leak located in the upper right quadrant of the bottom part of the reservoir. (e, f). Geometry and voltage distribution for a leak located in the upper right corner of the bottom part of the reservoir.

saturation of the silica sand was used to fill the reservoir. Several holes were drilled at the bottom of the reservoir to simulate the bottom leakages. Leaks with diameters of 0.4 cm, 0.6 cm, and 0.8 cm were used to evaluate the influence of leak size on the results. Three and five connected holes with the diameter of 0.4 cm were also used to study the effect of the shape of leaks (for instance to mimic the presence of a crack in the geomembrane).

2.2. *Mise-à-la-masse* experiments

The voltage responses with leaks at different locations on the bottom of the reservoir were measured in the *mise-à-la-masse* measurements. A total of 59 stainless steel electrodes (length, 0.7 cm; diameter, 0.3 cm) were placed at the top surface of the sand body around the reservoir. The positive (injection) current electrode (i.e., A) was set up at the top center of the water-filled reservoir, while the negative (return) current electrode (i.e., B) was located at the left center of the sand body surface (Fig. 1). The distributions of electrical potential

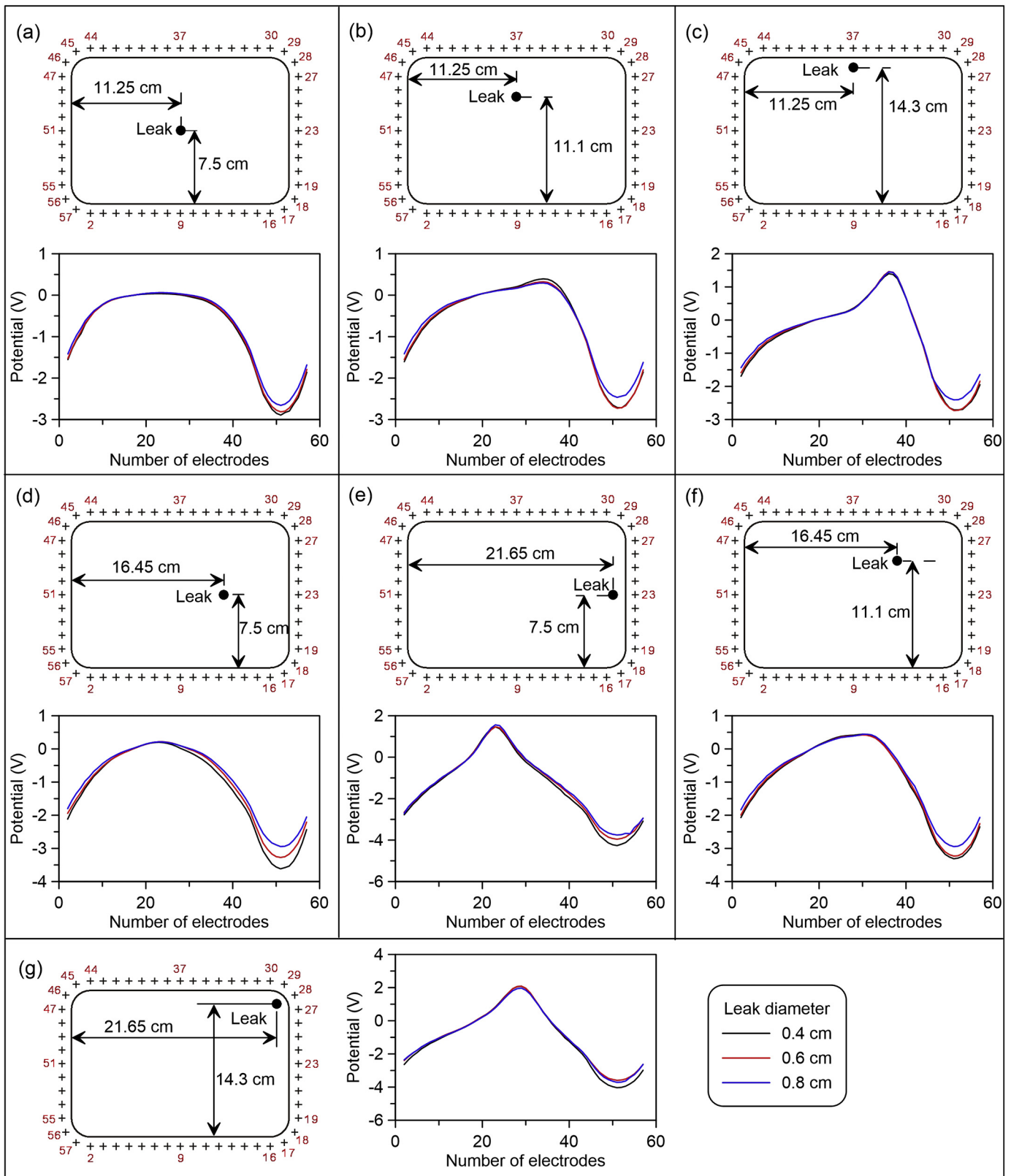


Fig. 3. The variations in the electrical potential measured in the sandbox experiment with a single leak (physical experiments). For each part, the first figure shows the location of the leak, and the second figure shows the variations in the electrical potential measured by the surrounding electrodes. The black, red, and blue lines denote the potential responses of leak with leak diameters of 0.4 cm, 0.6 cm, and 0.8 cm, respectively. (For interpretation of the references to colour in this figure legend, the reader is referred to the web version of this article.)

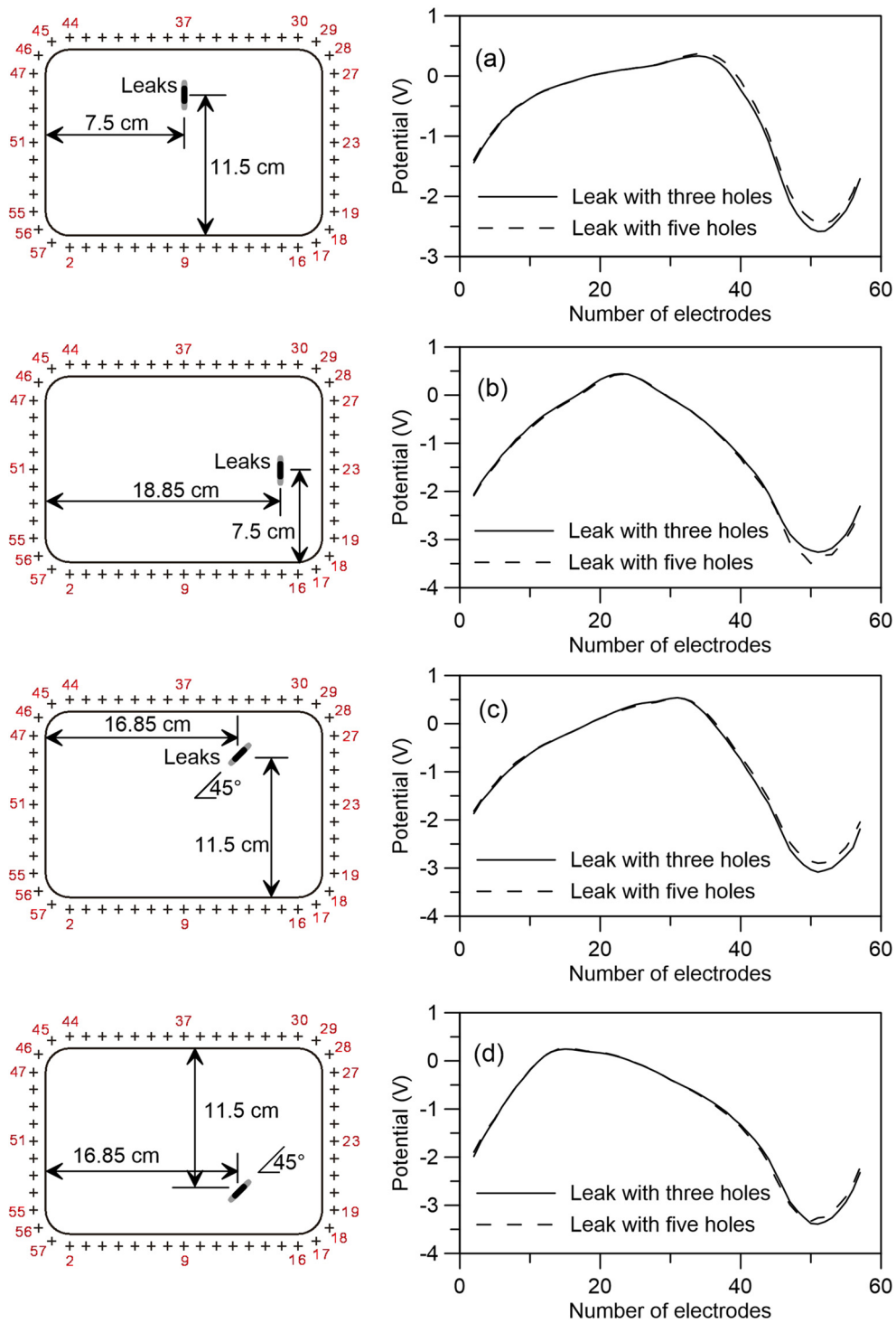


Fig. 4. The variations in the electrical potential with three and five connected holes used to model the crack leak (physical experiments). The holes have a diameter of 0.4 cm. For each part, the left figure shows the location of leak, and the right figure shows the variations in the electrical potential. The solid and dashed curves denote the potential responses of the leak with three and five connected holes, respectively. The difference between the two curves is very small.

relative to the reference electrode (i.e., N), which was placed at the right bottom corner, were measured with the remaining 56 scanning electrodes (i.e., M_i , i from 1 to 56). These scanning electrodes were organized around the reservoir. The distance between the scanning electrodes and the reservoir boundary was 1 cm. The scanning electrodes were set equidistantly on each side of the reservoir. The electrode spacings along the long and short sides were 1.357 cm and 1.57 cm, respectively. A polyvinyl chloride framework was used to fasten all of the electrodes so that they were kept at the constant

locations. The mise-à-la-masse measurements were carried out with a resistivity meter (ABEM Terrameter SAS-1000, Sweden). The supply current I was set at 20 mA. The data sets including the electrical voltage differences and corresponding standard deviations were logged automatically. In each data set, there were 56 voltage data and corresponding standard deviations.

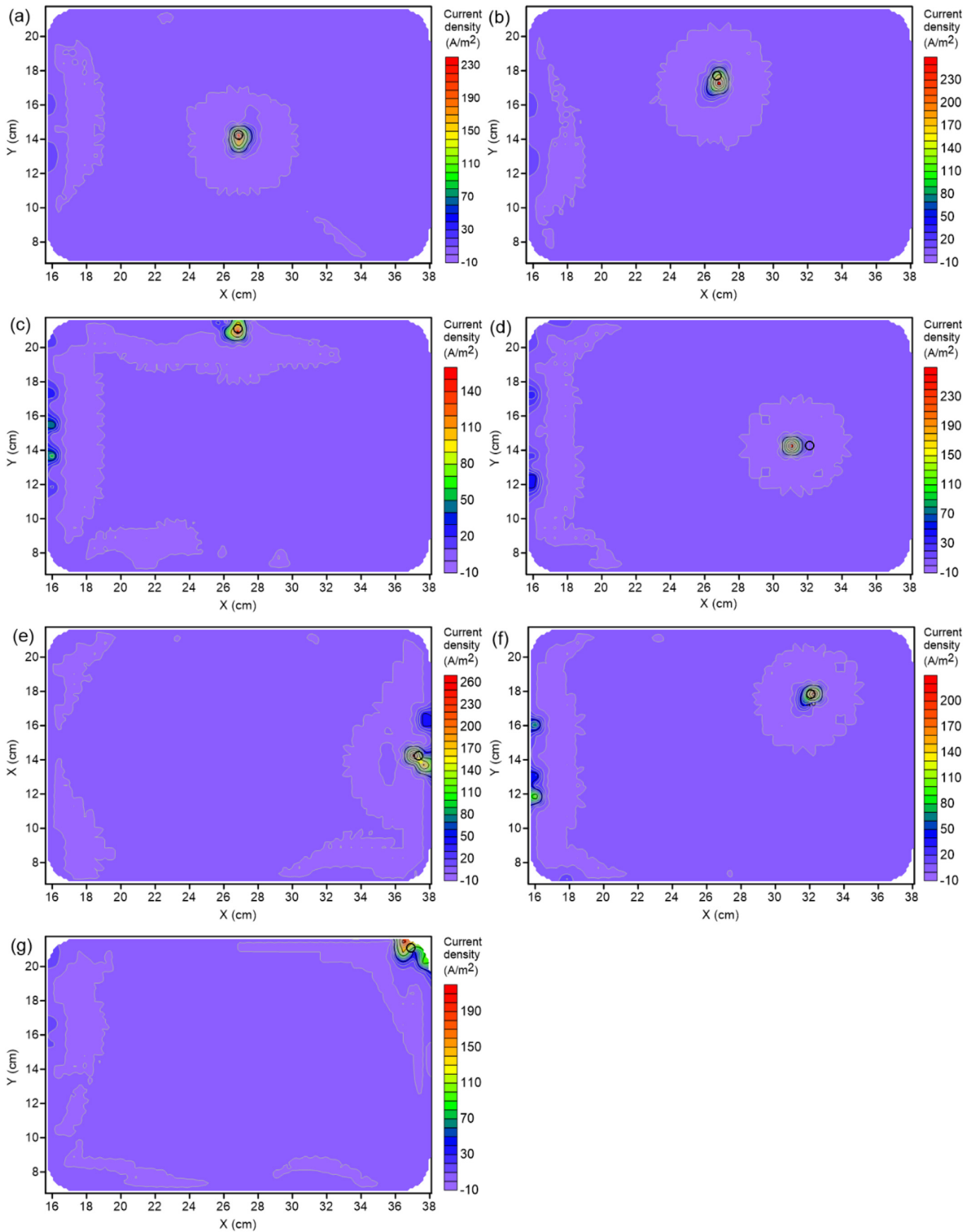


Fig. 5. Distributions of source current density for a single leak at different locations (physical experiments). The black open circles denote the location of leak. Leaks with the diameter of 0.6 cm are used in both the physical experiments and simulation models. The simulation model is used to obtain the kernel matrix (K) in Eq. (4). The inversion results show the accurate locations of leak with the maximum of current density are identified.

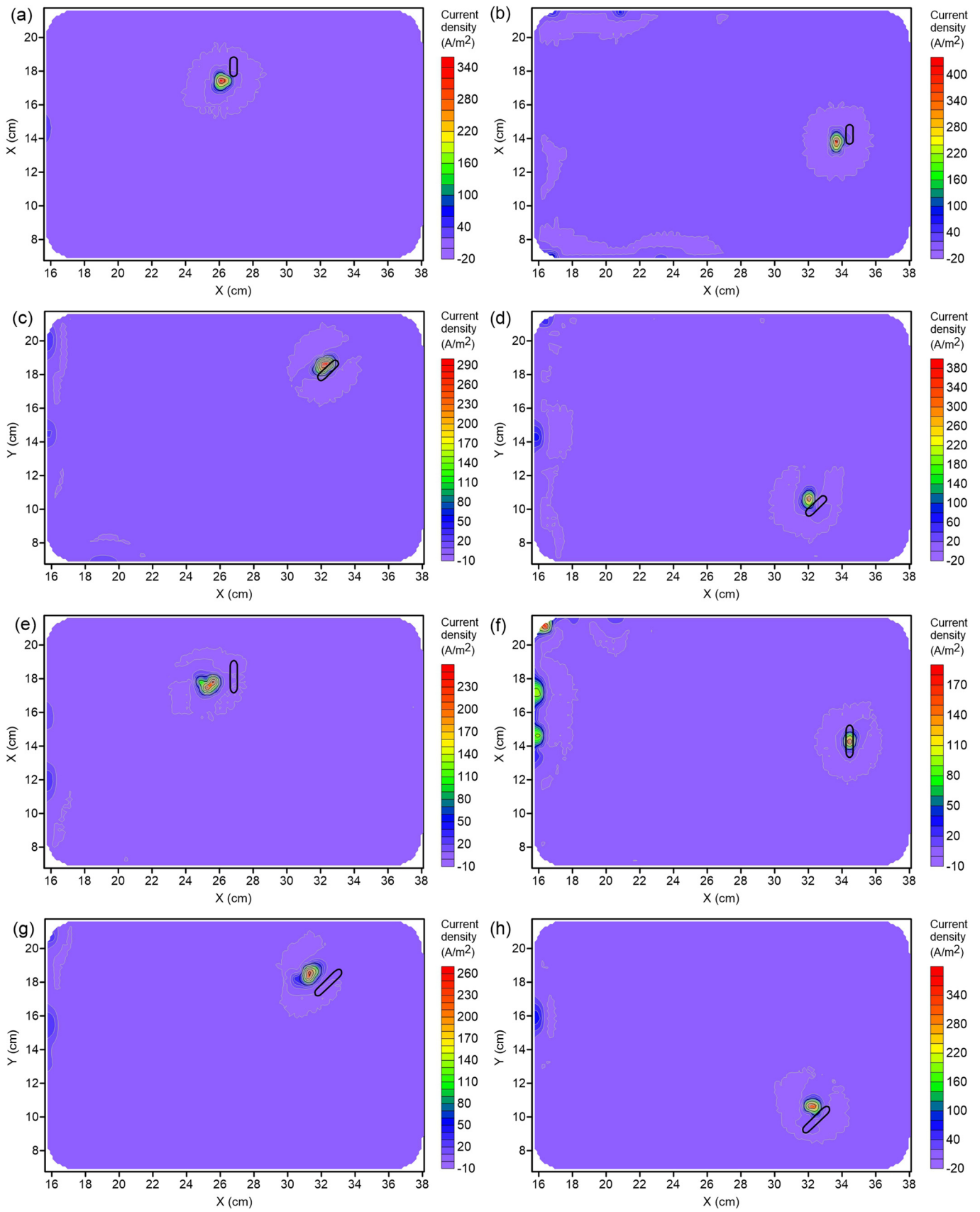


Fig. 6. Distributions of source current density for three and five connected holes at different locations (physical experiments). The small black open curves denote the locations of leak. The inversion results for three connected holes are shown in (a)–(d), while the inversion results of five connected holes are shown in (e)–(h). The holes with a diameter of 0.4 cm are used in both the simulation models and physical experiments. All of the crack leaks are detected, although there are some deviations.

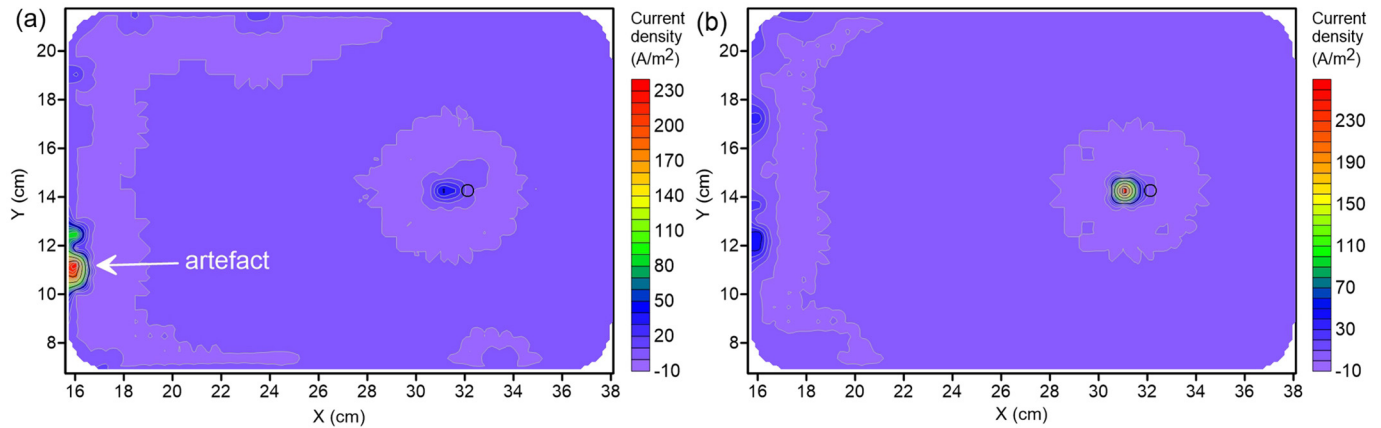


Fig. 7. Comparison of inversion results with the initial mean model (a) and predefined model (b) according to Eqs. (1) and (2). The black open circles denote the locations of leak. For the inversion results based on initial mean model, an artefact with the maximum value of current density appears in the left lower part. The inversion results with a predefined model according to Eqs. (1) and (2) perform better than that with an initial mean model.

2.3. Forward and inverse modeling

Forward and inverse modeling steps were used to localize the locations of the bottom leaks. First, the mise-à-la-masse measurement was simulated with forward modeling by solving the corresponding elliptic partial differential equation according to the approach described in details in Ling et al., (2019). Values of Green's functions containing the measured electrical potential differences with the bottom leak at various locations were collected by the forward modeling. Values of Green's functions are expressed in a kernel matrix, which is used in the inverse modeling as a forward operator. In the kernel matrix, there are 56 rows corresponding to the potential stations. Each column of the kernel matrix contains the measured electrical potential differences with the bottom leak at a certain location. Because three sizes of leaks (i.e., diameters of 0.4 cm, 0.6 cm, and 0.8 cm) were used in the physical experiments, the forward modeling was conducted three times to obtain the corresponding kernel matrixes. For leaks with diameters of 0.4 cm, 0.6 cm, and 0.8 cm, the bottom of the reservoir was subdivided into 2023, 913, and 459 cells, respectively. Hence, the dimensions of kernel matrixes for the leak with diameters of 0.4 cm, 0.6 cm, and 0.8 cm are 56×2023 , 56×913 , and 56×459 , respectively. In addition, we tested the performance of traditional protocols by arranging the scanning potential electrodes (N) on the bottom inside the reservoir (Frangos, 1997).

In the second step, an inversion method similar to the self-potential inversion method was used (Jardani et al., 2008; Soueid Ahmed et al., 2013; Haas et al., 2013). An objective function, which includes a data misfit term and a regularization term, is subject to minimization using Tikhonov regularization (see Tikhonov and Arsenin, 1977). A penalty function including a depth-weighting matrix and minimum support function was also used in the inverse modeling in order to localize the leak (Zhdanov and Tolstaya, 2004; Mao and Revil, 2016; Ling et al., 2019 for details). In the inversion results, the distributions of electrical current density on the bottom of the reservoir were obtained. The maximum values of source current density denote the estimated positions of leaks.

In Ling et al. (2019), the initial model with uniform current density distribution was used. We found the inversion based on the initial uniform model could generate several artefacts when the measured potential signal is weak and in presence of noise. In order to propose a more robust approach, we define an initial model based on the distribution of root mean square between the observation and simulation data. The root mean square R and the initial model parameters (\mathbf{m}^0) are defined as.

$$R_i = \sqrt{\frac{\sum_{j=1}^n (K_{ji}I - \psi_j)^2}{n}} \quad i = 1, 2, \dots, m \quad (1)$$

$$m_i^0 = \frac{1}{R_i} / \sum_{i=1}^m \left(\frac{1}{R_i} \right) \quad i = 1, 2, \dots, m \quad (2)$$

where I denotes the injected current (20 mA for our sandbox experiment). K_{ji} , the element of the kernel matrix, is the voltage response at the j th voltage station due to the leak located at the i th cell. ψ_j is the observed electrical potential at the j th voltage station in the physical experiments. m is the number of discretized cells comprising the bottom of reservoirs, while n is the number of measured voltage stations. The root mean square R is a measure of the imperfection of the fit of the simulation data to the observation data. The initial model parameter (m_i^0) at each cell is inversely proportional to the root mean square value between the observation and simulation data by assuming the leak locating at the corresponding cell. The normalization was then carried out to obtain the initial model parameters, which improve the inversion results (see Discussion section below).

3. Laboratory experimental results

3.1. Distribution of measured potential differences

In electrical measurements for leak detection, the potential electrodes are usually placed inside or outside of the geomembranes. The positive current electrode A and negative current electrode B are located inside and outside the reservoir, respectively, in order to force the current to focus through the leaks. When the reference potential electrode N is located outside the reservoir, the extrema in the electrical potential distribution underline the position of the leaks (see Frangos, 1997). We tested the performance of this method with a synthetic experiment. Fig. 2 shows the location of the leak and the corresponding contour maps of voltage by placing the scanning electrodes (see the crosses) inside the reservoir. The results show that the minima of the potential distribution are indeed close to the true locations of the leaks. This method is therefore efficient and simple to detect leaks in the case where the electrodes can be installed inside the bottom of the reservoir. However, sometimes the bottom of the reservoir is not accessible and this for various reasons. In these cases, the only way is to setup the electrodes around the reservoir and conduct remote measurements with the hope to detect the leak. This is this situation we are mostly interested in the present case.

The potential difference distributions obtained around the reservoir with a single leak in the physical experiments are presented in Fig. 3. The true locations of leaks are also shown. Because the negative current

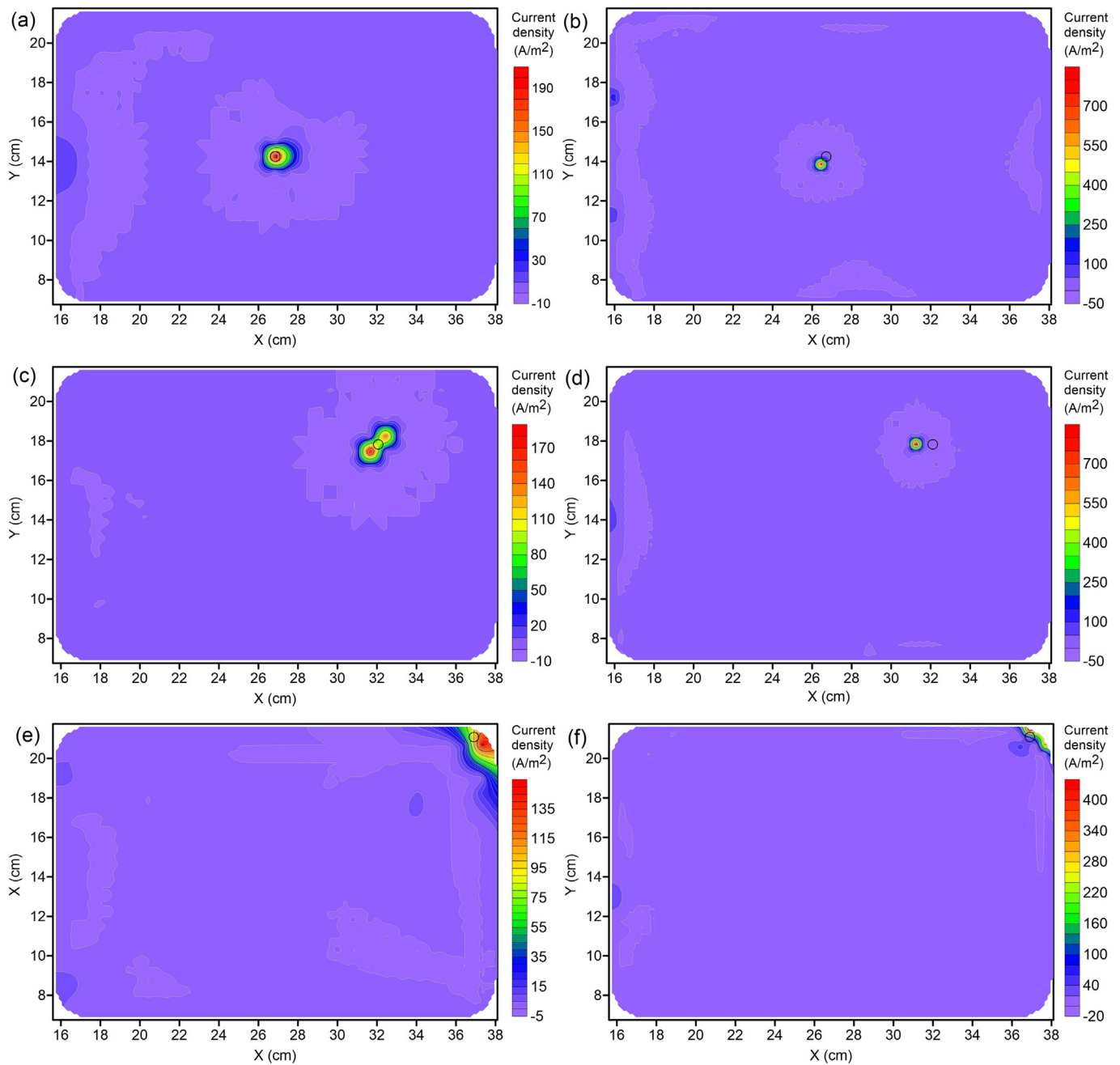


Fig. 8. Comparison of current density distribution for a single leak at different locations (physical experiments). The black open circles denote the locations of leak. Note that the inversion algorithm cannot retrieve the true size of the leak. In figure a, c, and e, leaks with diameters of 0.4 cm and 0.8 cm are used in the physical experiments and simulation models, respectively. On contrary, in figure b, d, and f, leaks with diameters of 0.8 cm and 0.4 cm are used in the physical experiments and simulation models, respectively.

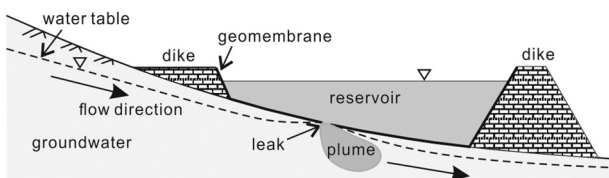


Fig. 9. Schematic diagram of the pollution plume migration due to the bottom leak of a reservoir for storing saline (Zheng and Bennett, 2002). The saline plume spreads with the groundwater flow.

electrode (B) and reference potential electrode (N) are located on the left and right hand of the layout, the measured potential differences generally decrease from the right to the left of reservoir. Compared to the reservoir side leaks investigated by Ling et al. (2019), the case corresponding to the bottom leaks generates weak electrical signals, which makes harder the localization of the bottom leak. When the leak is located in the center of the bottom side of the reservoir, the maximum of voltages is less than 0.1 V (Fig. 3a). The maximum voltage of scanning electrodes increases with the decrease from the leak. When the leak is located in the upper right corner, the maximum of voltages reaches about 2.0 V (Fig. 3g). The differences of voltage between three sizes of leaks (i.e., diameters of 0.4 cm, 0.6 cm, and 0.8 cm) are overall small.

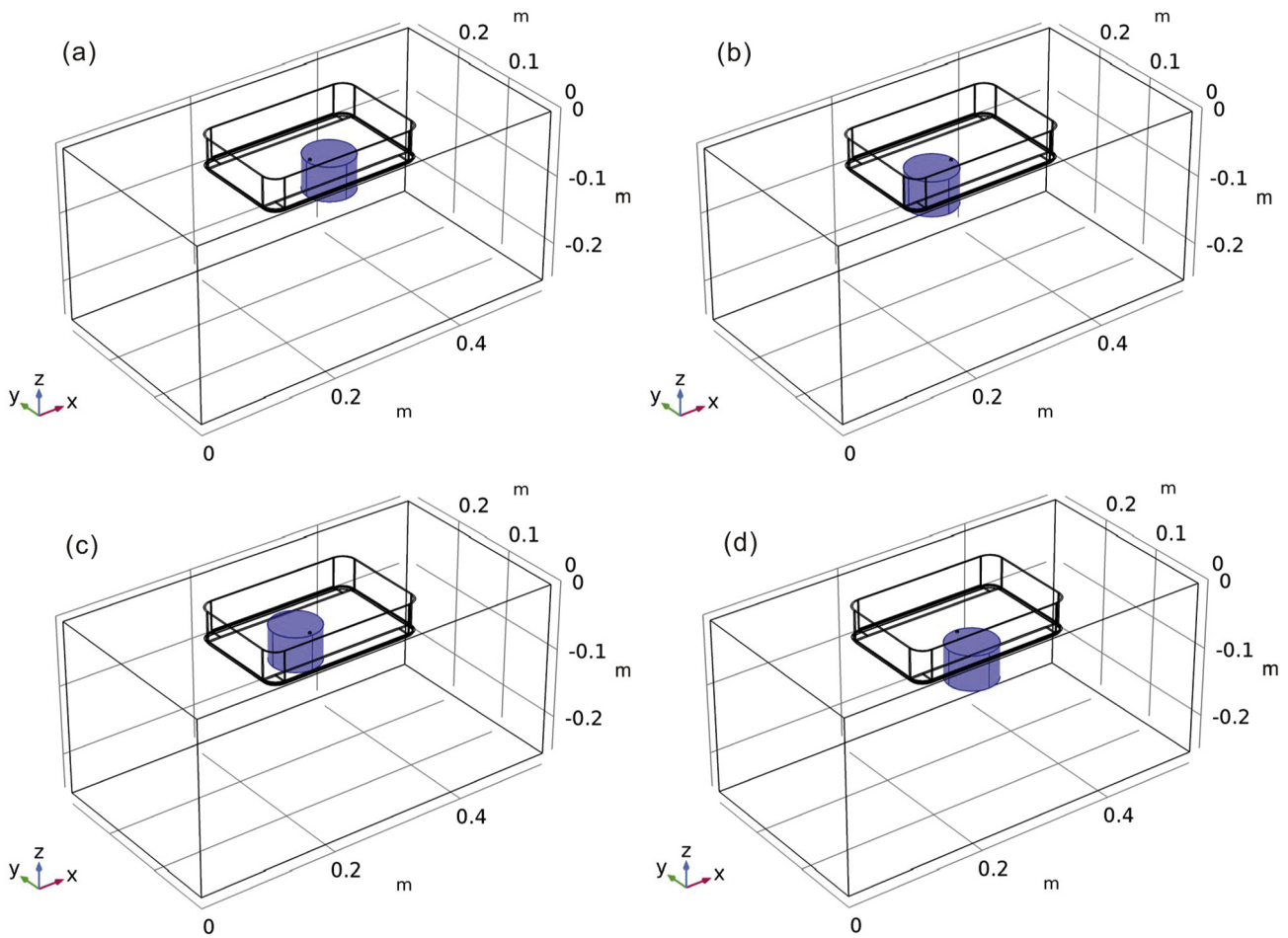


Fig. 10. The locations of a conductive zone under the leak (synthetic experiments). A conductive zone (purple colour) with a diameter of 7.0 cm and a height of 5.0 cm was used to analyze the effect of the undetected conductive zone on the inversion results. The resistivity of $5 \Omega \text{ m}$ was assigned to the conductive zone. The conductive zone was offset by 3.0 cm along the +X direction (a), -X direction (b), +Y direction (c), and -Y direction (d). (For interpretation of the references to colour in this figure legend, the reader is referred to the web version of this article.)

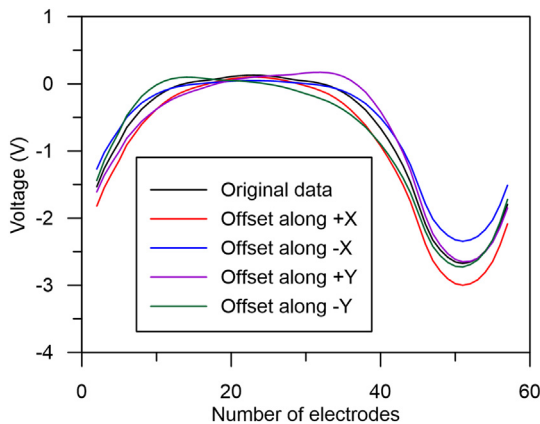


Fig. 11. The variations in the electrical potential for the single leak without the conductive zone and with the offset conductive zones (synthetic experiments). The offset conductive zones obviously distort the voltage curves by increasing the voltage measured by the closer electrodes.

We also test the case of a leak with a crack shape, which can be due to the mechanical rupture of the geomembrane over time. The connected holes with the diameter of 0.4 cm are used in the physical experiments. The potential difference distribution with three and five connected holes are shown in Fig. 4. For three connected holes, the leak has dimensions of a length of 1.2 cm and a width of 0.4 cm. For five

connected holes, the leak has a length of 2.0 cm and a width of 0.4 cm. In Fig. 4, the left figure shows the location of the leak, and the right figure shows the variations in the electrical potential distribution. The potential of the closest electrode is the maximum value, and other values decrease with the increase of the distance between the leak and electrodes. The differences of the electrical potential between the three and five connected holes are small, the average absolute value of which is only 0.05 V.

3.2. Evaluation of leaks

The inversion results of leaks with diameters of 0.4 cm, 0.6 cm, and 0.8 cm are similar. Due to the space limitation, only the distributions of source current density for a single leak with the diameter of 0.6 cm are shown in Fig. 5. Leaks with the diameter of 0.6 cm are used in both the physical experiments and simulation models. The simulation model is used to obtain the kernel matrix (K) in Eq. (4). In the inversion results, the maximum values of current density denote the leakage. The average bias between the real positions and evaluation results of a single leak is 0.43 cm, and the maximum bias is 1.0 cm. It is obvious that the inversion algorithm overall identifies the accurate locations for a single leak.

We used several connected holes with a diameter of 0.4 cm to model a leaking crack. The leak with the diameter of 0.4 cm are used in the simulation model to obtain the kernel matrix (K). The distributions of source current density for three and five connected holes at different locations are presented in Fig. 6. The inversion results for three

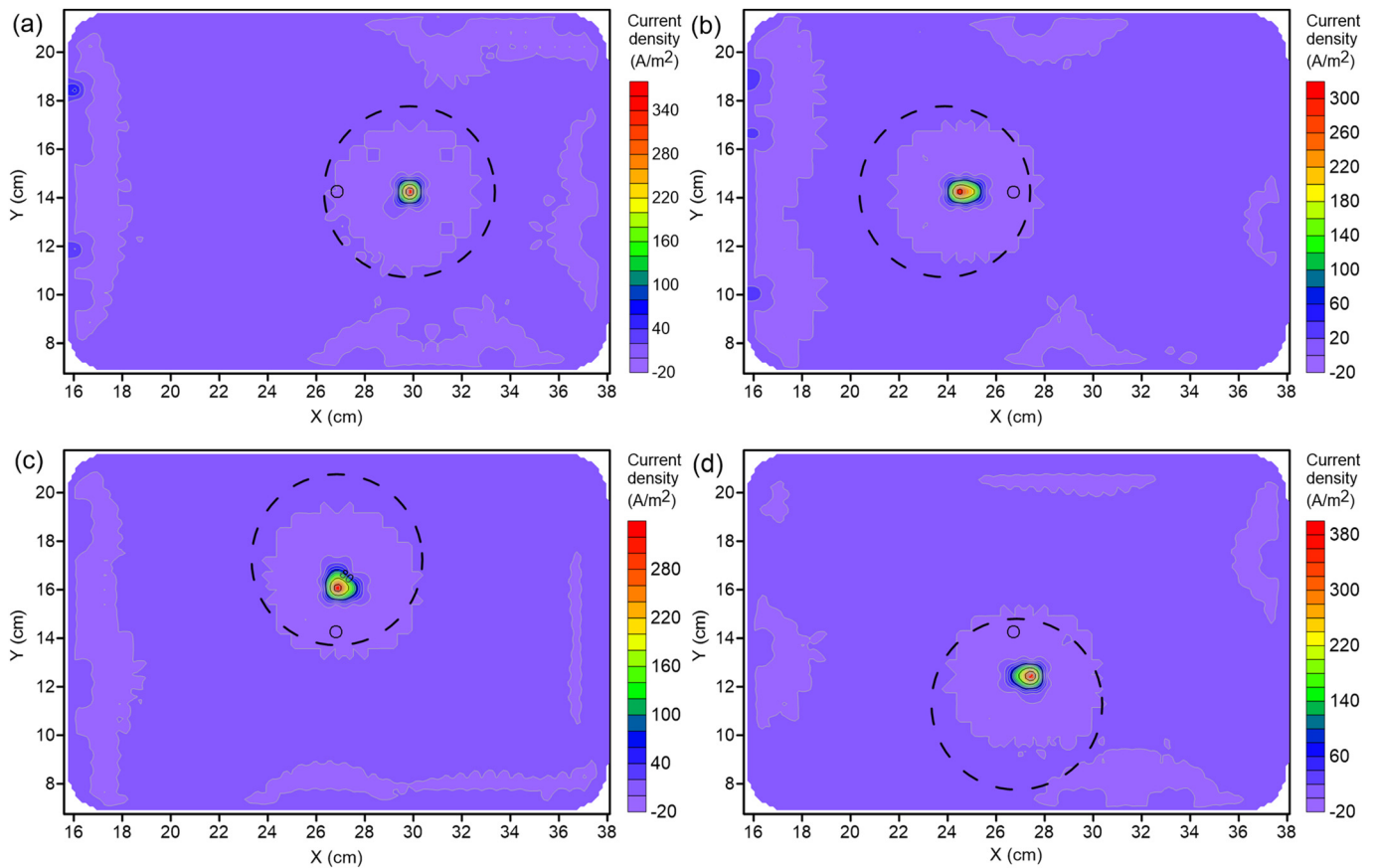


Fig. 12. The effect of the undetected conductive zone on the evaluation results (synthetic experiments). The black open circles denote the location of leak. The black dashed open circles denote the locations of the undetected conductive zone.

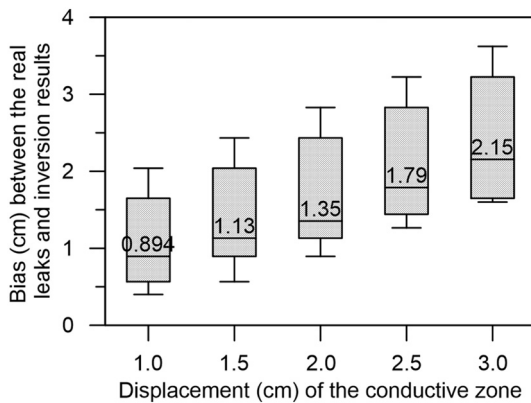


Fig. 13. The relationship between the displacements of conductive zone and the inversion biases (synthetic experiments). A conductive zone with a diameter of 7.0 cm and a height of 5.0 cm was used to analyze the effect of the undetected conductive zone on the inversion results. The resistivity of 5Ωm was assigned to the conductive zone. The median values are labeled. The inversion biases increase with the displacement of the conductive zone.

connected holes are shown in Fig. 6(a)–(d), while the inversion results of five connected holes are given in Fig. 6(e)–(h). For the three connected leaks, the average, minimum, and maximum biases between the real positions and evaluation results of leaks are 0.62 cm, 0.28 cm, and 0.80 cm, respectively. The bias increases with the length of the crack leak. For the five connected leaks, the average, minimum, and maximum biases between the real positions and evaluation results of leaks are 0.98 cm, 0.57 cm, and 1.20 cm, respectively. It is found that the shapes of crack leaks are not well reflected in the inversion results. We

attribute the poor identification of crack shape to the minimum support function used in the inversion algorithm.

4. Result and interpretation of the sandbox experiments

4.1. The effect of initial models on the inversion results

For the bottom leakage detection of a reservoir, the initial model plays an important role in the inversion processes due to the weak signals. The data of Fig. 3(d) were used to show the difference of the inversion result based on different initial models. In Fig. 3(d), the leak is located in the middle right, and the maximum of voltage is only 0.2 V. We first inverted the data with the initial mean model used by Ling et al. (2019). The inversion result based on the initial mean model is shown in Fig. 7(a). An artefact with the maximum value of current density appears in the left lower part, while the current density at the real position is not obvious. In this study, we proposed an initial model based on the distribution of root mean square values between the measured data and simulation data, see Eqs. (1) and (2) for details. The inversion result is shown in Fig. 7b. Comparison of inversion results with the two kinds of initial models shows that the predefined initial model based on the distribution of root mean square values between the measurement and simulation data improves the inversion results greatly. The artefacts are suppressed significantly. In fact, there are still several artefacts appearing in the left lower part in Fig. 7(b). The leak at the left center part would generate potential signals close to zero volt. When there were some misfits between the measured and simulation potentials, the inversion algorithm leads to the occurrence of several spurious current sources in the left center part of the domain to decrease the misfit.

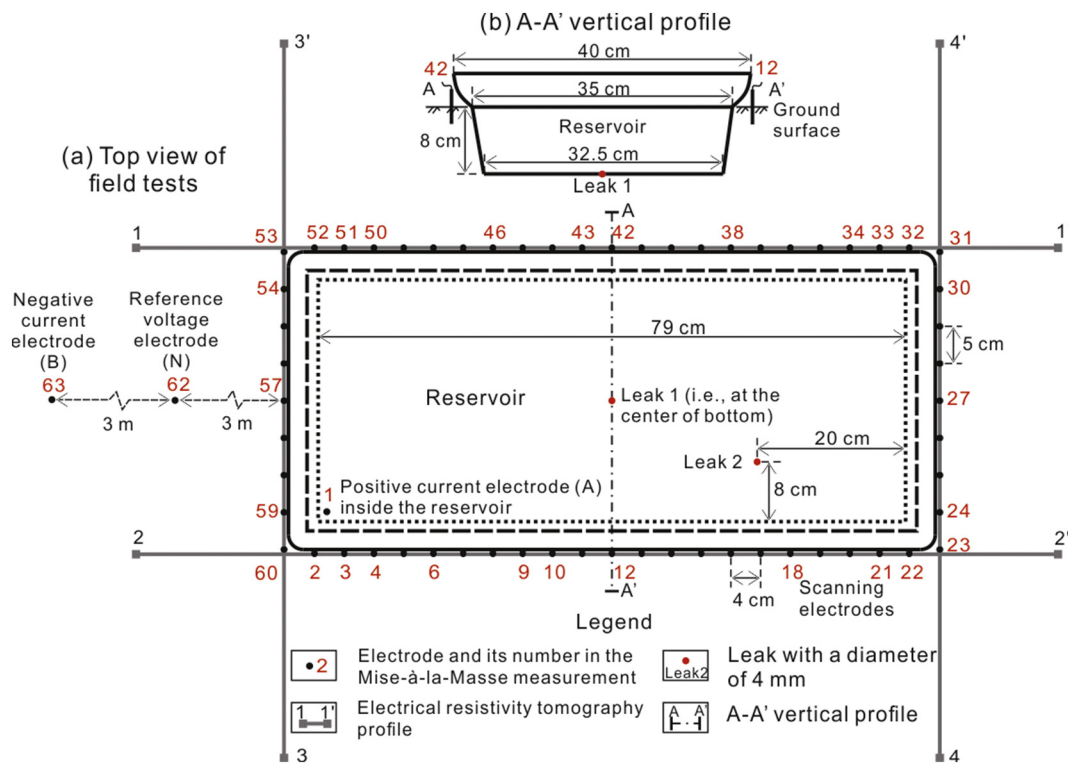


Fig. 14. The layout of field tests for the leak detection. In the resistivity measurements, four profiles are arranged around the reservoir (e.g., 1–1' profile). In the mise-à-la-masse measurement, the positive (A) and negative (B) current electrodes are located inside and outside of the reservoir. 60 scanning voltage electrodes are organized around the reservoir, and the reference voltage electrode (N) is located between the negative current electrode and the reservoir.

4.2. The effect of leak size in forward modeling on the inversion results

Before the inversion modeling, the forward modeling is carried out to obtain the kernel matrix (K). The size of the leak has to be set in the forward modeling. In application, the actual size of the leak is usually unknown. Hence, it is a common situation to use an unmatched size of the leak in the forward modeling. Ling et al. (2019) analyzed the leak detection on the side faces of a reservoir with the same algorithm. They found that the inversion algorithm underestimates the depth of large leaks while it overestimates the depth of small leaks. For the bottom leakage detection of the reservoir, in order to test the performance of inversion algorithm, the kernel matrix (K) from forward modeling with leaks of 0.8 cm diameter was used to evaluate the position of leaks of 0.4 cm diameter (Fig. 8a). The opposite situation was also tested (Fig. 8b). All of leaks are fairly-well identified. We ascribe this phenomenon to the weak electrical potentials (Fig. 3) and the insensitivity of potential to the size of leak.

4.3. Effect of an undetected conductive zone

The electrical resistivity distributions of the ground around and under the reservoir have to be given in the forward modeling. The distribution of electrical resistivity can be obtained with the resistivity measurement and available geological information. Additionally, the effect of leak on the resistivity distributions of soil should be considered. The leakage of the reservoir with waste water can last long enough before it is perceived through the unbalance of water quantity or the obvious deterioration of surrounding groundwater environment. For a water reservoir, the leakage could increase the water content of surrounding soil. For a reservoir or pond filled with saline water, its leakage can increase the salinity of surrounding groundwater. The resulting plume would migrate in the groundwater changing the electrical conductivity distribution (Fig. 9).

To further investigate the influence of undetected conductive zone

around the leak on the inversion results, an artificial conductive zone with the dimensions of 7.0 cm diameter and 5.0 cm height was added under the leak in the synthetic experiments. The ratio of resistivity between the background and the conductive zone was set 10:1. The conductive zone was assigned with the resistivity of 5 Ωm. The conductive zone was offset by 3.0 cm along the +X, -X, +Y, and -Y directions (Fig. 10). The variations in the electrical potential for the single leak without conductive zone and with the offset conductive zones are shown in Fig. 11. The offset conductive zones obviously distort the voltage curves by increasing the voltage measured by the closer electrodes. The simulated potential data were then contaminated with a white noise level of a maximum of 5% before proceeding to the inversion algorithm. The inversion results are presented in Fig. 12. The black dashed open circles denote the locations of undetected conductive zone. It is obvious that the evaluated positions (i.e., maximum values of current density) of leaks approach the conductive zone.

To evaluate the effect of conductive zone on the inversion results, we further carried out the synthetic simulation more than 200 times with the displacement of 1.0–3.0 cm, and then calculated the statistics of biases between the real leak and inversion results. The results are shown in Fig. 13. The biases increase with the displacement of the conductive zone, which means that the biased conductive zone due to the leak of water or saline may significantly distort the inversion results. In the field, to detect the accurate locations of the leak, it is therefore necessary to image the resistivity distribution through electrical resistivity tomography. If the forward modeling step in the analysis of the mise-à-la-masse method can include the electrical resistivity distribution, we expect an improvement in the detection of the leak.

5. Field tests

5.1. Materials and methods

In order to further test the performance of the mise-à-la-masse

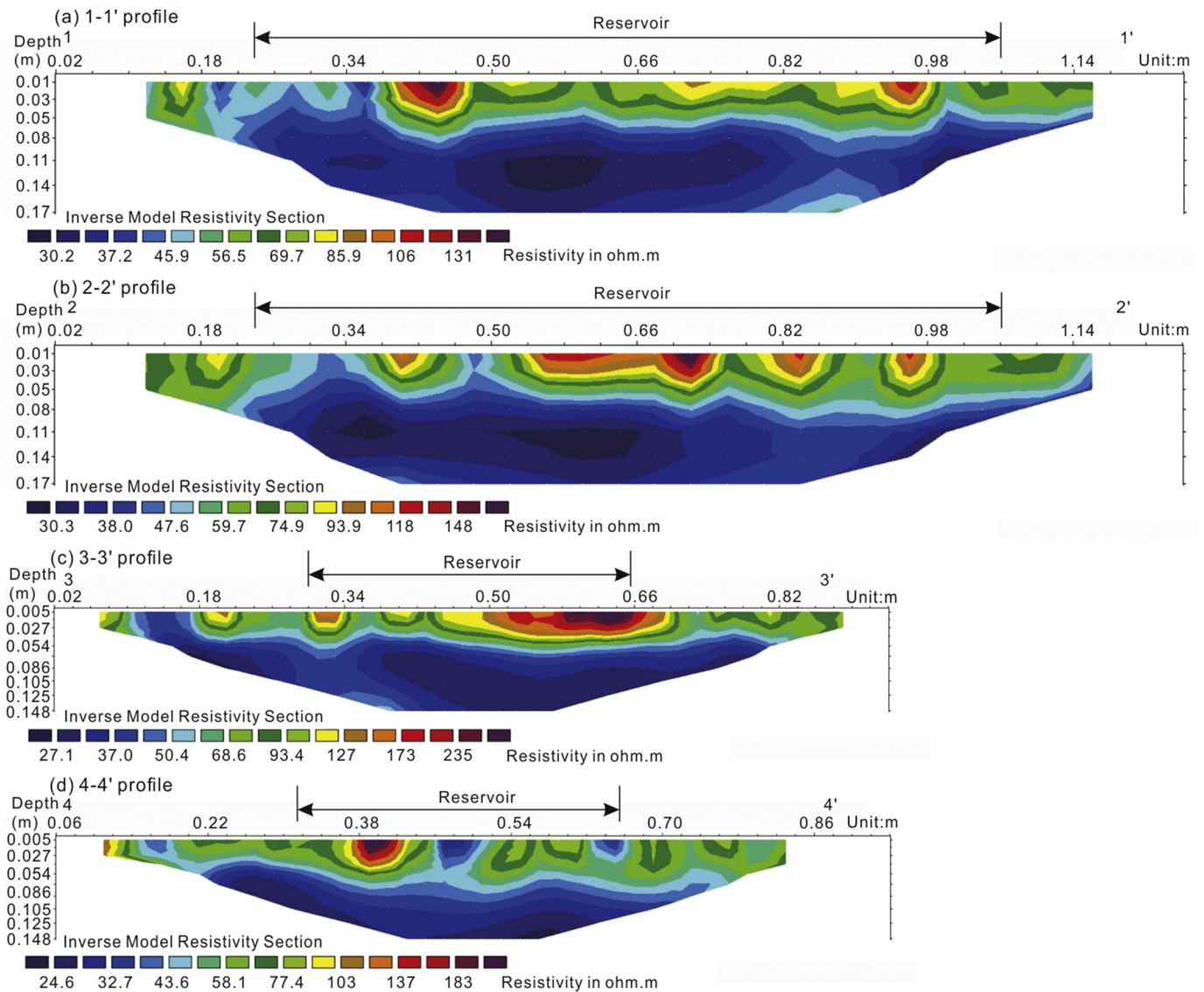


Fig. 15. Electrical resistivity tomography for the field test. The profiles show a shallow resistive layer to a depth of ~5 cm followed by a conductive soil.

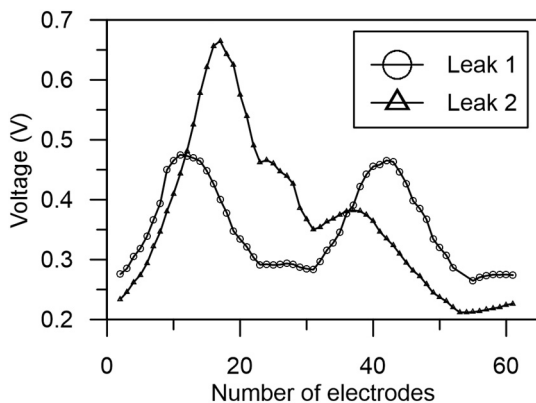


Fig. 16. The variations in the electrical potential difference measured in the field tests. The first leak is located at the center of the bottom, and the second leak is placed at the lower right part of the bottom of the tank (Fig. 14).

method in the leak detection, we carried out small-scale field tests in the campus of University Savoie Mont Blanc (Savoie, France). The surface of the test site is covered by a layer of silt- and clay-sized sediments mixed with gravels. A plastic cubic tank with the dimensions of

82 cm length, 35 cm width, and 13.5 cm height was used to simulate the water reservoir. The lower half of the reservoir was embedded in the ground (Fig. 14). Two leaks at the bottom were separately used. For one leak detection, the other leak was sealed during the measurement. The first leak is located at the center of the bottom. The second leak is located at the lower right of the bottom. The diameter of leak is 0.4 cm.

The distribution of electrical resistivity is one of the key factors influencing the leak detection. The Wenner array was used in this experiment. In order to obtain the distribution of resistivity, the resistivity measurements of four profiles were carried out before the mise-à-la-masse measurements. Two long profiles (i.e., 1-1' and 2-2') with 32 electrodes were placed along the two long sides of reservoir, while two short profiles (i.e., 3-3' and 4-4') with 24 electrodes were placed along the two short sides of reservoir. The electrode spacing was 4 cm. The apparent resistivity data were inverted using the Res2dinv software based on the least-squares method (Loke, 2007).

In the mise-à-la-masse measurement, a total of 63 steel electrodes were used. The positive current electrode A was placed at the lower left corner of the tank, while the negative current electrode B was placed at a 6 m distance from the tank. The reference voltage electrodes N was located between the tank and the negative current electrode B. A total of 60 scanning voltage electrodes (M) were placed around the tank. The

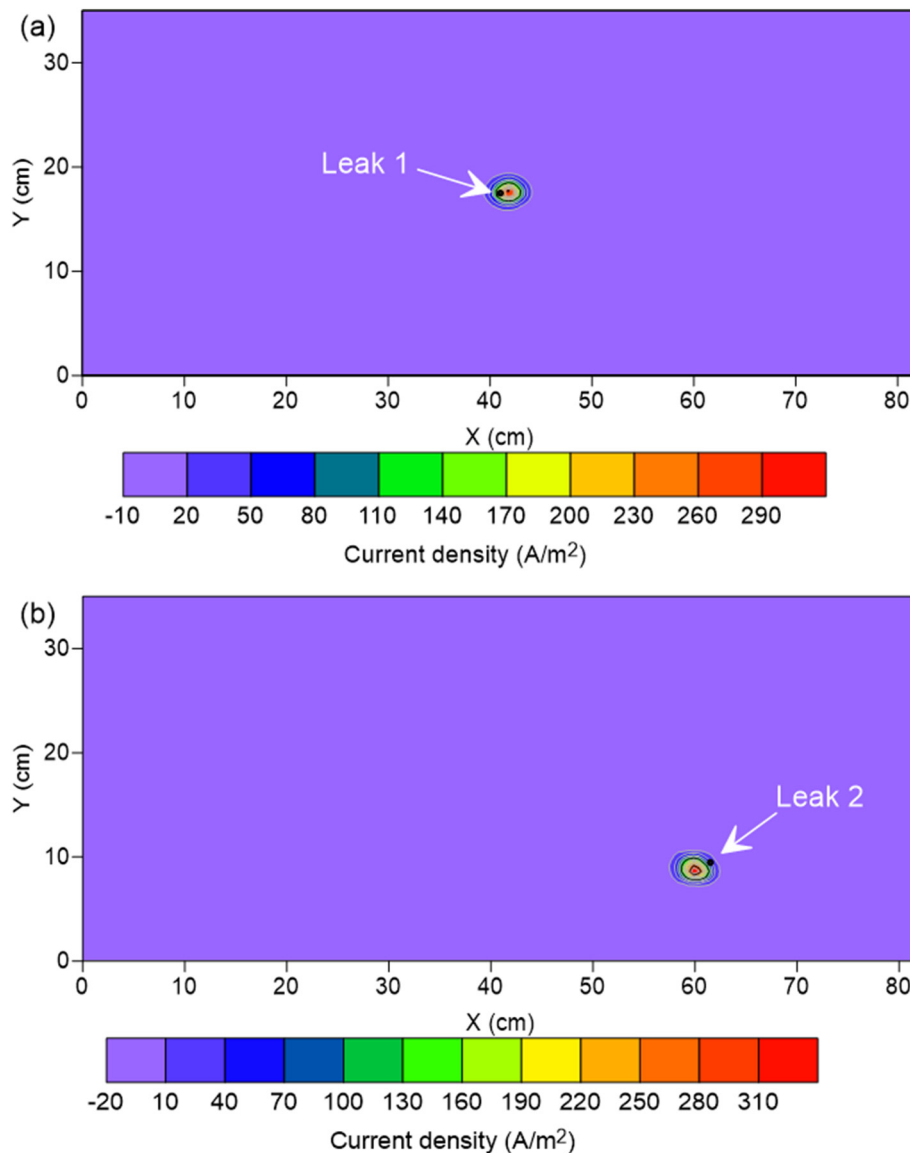


Fig. 17. Distributions of the source current density for leak detection in in the field tests. The true position of the leak is identified with the small filled circles. The leaks are properly identified with a precision of 1 cm.

spacings of electrodes are 4 cm and 5 cm along the long side and short side of the reservoir, respectively. An ABEM Terrameter SAS-1000 resistivity meter was used to carry out the resistivity and mise-à-la-masse measurements. The supply current I is set at 20 mA.

During the forward modeling, if we use the leak with a diameter of 0.4 cm, the bottom of the reservoir is subdivided into 17,661 cells. It takes more than 100 h with a normal computer (CPU: Intel core i7-4790 3.60 GHz, RAM: 32GB) to calculate the kernel matrix. Because the mise-à-la-masse method is not sensitive to the size of bottom leaks, we use the leak with a diameter of 1.0 cm, and the bottom of the reservoir is subdivided into 2763 cells. Leaks are then evaluated with the inversion method introduced in Section 2.3.

5.2. Results of the electrical resistivity profiles

The results of the four ERT profiles are shown in Fig. 15. The resistivity distributions are similar in four profiles. The soil resistivity decreases with the depth. A significant resistive layer (more than $50 \Omega\text{m}$) was found at approximately a depth of less than 5 cm. The resistivity of soil at the depth more than 5 cm generally varies at the range of $30\text{--}50 \Omega\text{m}$. The resistivity distributions from ERT

measurements were imported to the simulated forward model during the mise-à-la-masse data processing.

5.3. Distribution of measured potential differences

The potential differences measured around the reservoir in the field tests are shown in Fig. 16. When the leak (i.e., leak 1) is located at the center of the bottom, the maximum and minimum values of voltage differences are 0.47 V and 0.26 V, respectively. When the leak (i.e., leak 2) is located at the lower right part of the bottom (Fig. 14), the maximum and minimum values of voltage differences are 0.67 V and 0.21 V, respectively. With the measured potential differences, the positions of leaks are then evaluated by the Tikhonov regularization.

5.4. Evaluation of leaks

Distributions of the source current density for the leak detection are shown in Fig. 17. The maximum values indicate leaks. It is found that leaks are identified properly. For leak 1 with the coordinates of (41, 17.5), the evaluated position is (42, 17.5). For leak 2 with the coordinates of (60, 8.5), the evaluated position is (60, 9.5). The results

deviation is 1 cm, which is equal to the size of leak in the kernel matrix. The inversion results of the field data show that the mise-à-la-masse method is a promising approach to detect the bottom leak of reservoir, especially when it can be combined with electrical resistivity tomography.

6. Discussion

The accurate evaluation of electrical resistivity distribution is important for the mise-à-la-masse method used in the leak detection of reservoirs. In the field tests, both of the electrical resistivity tomography and mise-à-la-masse measurements were used altogether. Although the measurements may be time-consuming, the proposed method performs well. When the leakage of the reservoir usually lasts relatively long time, the joint inversion with geophysical methods and groundwater flow modeling could improve the leak detection and evaluate the influence scope of the leakage, which is the content of the next step.

7. Conclusions

Leakage of water-filled reservoirs could take place through geomembranes. The mise-à-la-masse method is here used to detect the leakage from the bottom of reservoirs using a set of electrodes localized at the ground surface just around the reservoir itself. A series of sandbox experiments were carried out to validate this method. In the forward modeling, the Green's functions are computed through numerical modeling to obtain the kernel matrix respecting the geometry of the electrode array and reservoir and the electrical resistivity distribution if known. The initial model parameters based on the distribution of root mean square values between the observation and simulation data are given to the inversion algorithm. In this algorithm, Tikhonov regularization including a weighting matrix and a minimum support method is used to strengthen the detection resolution of the leak(s) at the bottom of the reservoir.

A total of 29 sandbox experiments has been carried out. The results show that the inversion algorithm identifies the accurate locations for a single leak. For the leak associated with an elongated crack, the inversion algorithm is able to identify the correct location of the leak with a small bias. The error of inversion results increases with the length of the crack. We compare the inversion results based on the initial mean model and predefined model to show validation of the improved inversion strategy. The inversion result is poorly sensitive to the leak size used in the kernel matrix through forward modeling. In addition, we discussed the situation of long-term leakages from a reservoir leading to a conductive anomaly beneath the reservoir. When such conductive zone migrates, the resulting conductivity distribution may affect the recorded voltage distribution. The error of inversion results increases with the displacement of the conductive zone. Hence, the distribution of resistivity under the bottom of the reservoir should be considered in the inversion processes possibly through electrical resistivity tomography.

In addition, two small-scale field tests were conducted to further test the performance of the mise-à-la-masse method. Leaks are properly identified in these experiments. This study provides a suitable and efficient approach to detect the bottom leakage of reservoirs. The next step is to apply this approach to more complicated field studies.

Acknowledgements

This work is supported by the State Key Laboratory of Geohazard Prevention and Geoenvironment Protection Independent Research Project (SKLGP2018Z022). It is also supported by the project RESBA ALCOTRA funded by the European Community. We thank the editor and referee for the useful comments.

References

- Abdulsamad, F., Revil, A., Soueid Ahmed, A., Coperey, A., Karaoulis, M., Nicaise, S., Peyras, L., 2019. Induced polarization tomography applied to the detection and the monitoring of leaks in embankments. *Eng. Geol.* 254, 89–101. <https://doi.org/10.1016/j.enggeo.2019.04.001>.
- Binley, A., Daily, W., Ramirez, A., 1997. Detecting leaks from environmental barriers using electrical current imaging. *JEEG* 2 (1), 11–19. <https://doi.org/10.4133/JEEG2.1.11>.
- Colombo, A.F., Lee, P., Karney, B.W., 2009. A selective literature review of transient-based leak detection methods. *J. Hydro-Environ. Res.* 2 (4), 212–227. <https://doi.org/10.1016/j.jher.2009.02.003>.
- Daily, W., Ramirez, A., Binley, A., LaBrecque, D., 2004. Electrical resistance tomography. *Lead. Edge* 23 (5), 438–442.
- De Carlo, W., Perri, M.T., Caputo, M.C., Deiana, R., Vurro, M., Cassiani, G., 2013. Characterization of a dismissed landfill via electrical resistivity tomography and mise-à-la-masse method. *J. Appl. Geophys.* 98, 1–10. <https://doi.org/10.1016/j.jappgeo.2013.07.010>.
- Frangos, W., 1997. Electrical detection of leaks in lined waste disposal ponds. *Geophysics* 62 (6), 1737–1744. <https://doi.org/10.1190/1.1444274>.
- Francisco José, M., Fernando, D., Jesús, G., Wenceslao, M., Manuel, L., Lourdes, G., 2018. Identification of leakage and potential areas for internal erosion combining ERT and IP techniques at the Negratín Dam left abutment (Granada, Southern Spain). *Eng. Geol.* 240, 74–80. <https://doi.org/10.1016/j.enggeo.2018.04.012>.
- Haas, A.K., Revil, A., Karaoulis, M., Frash, L., Hampton, J., Gutierrez, M., Mooney, M., 2013. Electrical potential source localization reveals a borehole leak during hydraulic fracturing. *Geophysics* 78 (2), D93–D113. <https://doi.org/10.1190/GEO2012-0388.1>.
- Himi, M., Casado, I., Sendros, A., Lovera, R., Rivero, L., Casas, A., 2018. Assessing preferential seepage and monitoring mortar injection through an earthen dam settled over a gypsiferous substrate using combined geophysical methods. *Eng. Geol.* 246, 212–221. <https://doi.org/10.1016/j.enggeo.2018.10.002>.
- Jardani, A., Revil, A., Bolève, A., Dupont, J.P., 2008. Three-dimensional inversion of self-potential data used to constrain the pattern of groundwater flow in geothermal fields. *J. Geophys. Res. Sol. Ea.* 113 (B9), B09204. <https://doi.org/10.1029/2007JB005302>.
- Ketola, M., 1972. Some points of view concerning mise-à-la-masse measurements. *Geoexploration* 10 (1), 1–21. [https://doi.org/10.1016/0016-7142\(72\)90010-5](https://doi.org/10.1016/0016-7142(72)90010-5).
- Khan, A.A., Cunat, P., Beck, Y.L., Mars, J., Vrabie, V., Fabre, J.P., 2010. Distributed fiber optic temperature sensors for leakage detection hydraulic structures. In: 5th World Conference on Structural Control and Monitoring (5WCSCM). Proceedings of 5WCSCM, Tokyo, Japan, pp. 10071 Jul 2010.
- Lee, J.Y., Choi, Y.K., Kim, H.S., Yun, S.T., 2005. Hydrologic characteristics of a large rockfill dam: implications for water leakage. *Eng. Geol.* 80, 43–59. <https://doi.org/10.1016/j.enggeo.2005.03.002>.
- Ling, C., Revil, A., Abdulsamad, F., Qi, Y., Soueid Ahmed, A., Shi, P., Nicaise, S., Peyras, L., 2019. Leakage detection of water reservoirs using a Mise-à-la-Masse approach. *J. Hydrol.* 572, 51–65. <https://doi.org/10.1016/j.jhydrol.2019.02.046>.
- Loke, M.H., 2007. *Res2dinv, Rapid 2-D Resistivity and IP Inversion Using the Least-Squares Method – user's Manual*.
- Mao, D., Revil, A., 2016. Induced polarization response of porous media with metallic particles – part 3: a new approach to time-domain induced polarization tomography. *Geophysics* 81 (4), D345–D357. <https://doi.org/10.1190/geo2015-0283.1>.
- Mostafa, M.K., Ighere, J.O., Chawla, R.C., Peters, R.W., 2016. Groundwater protection and remediation. In: Chen, D.H. (Ed.), *Sustainable Water Management and Technologies*. Taylor & Francis Group, LLC, pp. 53–78.
- Musthafa, N.H.B., Hooi, Y.K., Hanssan, M.F., Shariff, A.M., Khalid, K.S., 2017. Automatic statistical inventory reconciliation for leak detection of petrochemical storage. *J. Comput. Theor. Nanos.* 23 (11), 10777–10781. <https://doi.org/10.1166/asl.2017.10151>.
- O'Connor, K.M., Dowding, C.H., 1999. *Geomeasurements by Pulsing TDR Cables and Probes*. CRC Press.
- Pant, S.R., 2004. Tracing groundwater flow by mise-à-la-masse measurement of injected saltwater. *JEEG* 9 (3), 155–165. <https://doi.org/10.4133/JEEG9.3.155>.
- Panthulu, T.V., Krishnaiah, C., Shirke, J.M., 2001. Detection of seepage paths in earth dams using self-potential and electrical resistivity methods. *Eng. Geol.* 59, 281–295.
- Perri, M.T., De Vita, P., Masciale, R., Portoghese, I., Chirico, G.B., Cassiani, G., 2018. Time-lapse mise-à-la-masse measurements and modeling for tracer test monitoring in a shallow aquifer. *J. Hydrol.* 561, 461–477. <https://doi.org/10.1016/j.jhydrol.2017.11.013>.
- Peyras, L., Royet, P., Deroo, L., Albert, R., Becue, J.-P., Aigouy, S., Bourdarot, E., Loudiere, D., Kovarik, J.-B., 2008. French recommendations for limit-state analytical review of gravity dam stability. *Eur. J. Environ. Civ. Eng.* 12 (9–10), 1137–1164. <https://doi.org/10.1080/19648189.2008.9693071>.
- Poulain, D., Peyras, L., Mériaux, P., 2011. Feedback and guidelines for geomembrane lining systems of mountain reservoirs in France. *Geotext. Geomembr.* 29 (4), 415–424. <https://doi.org/10.1016/j.geotextmem.2010.12.002>.
- Ramirez, A., Daily, W., Binley, A., LaBrecque, D., Roelant, D., 1996. Detection of leaks in underground storage tanks using electrical resistance methods. *J. Environ. Eng. Geophys.* 1 (3), 189–203. <https://doi.org/10.4133/jee1.3.189>.
- Revil, A., Jardani, A., 2013. *The Self-Potential Method, Theory and Applications in Environmental Geosciences*. Cambridge University Press (July 2013).
- Rozycki, A., 2009. Evaluation of the streaming potential effect of piping phenomena using a finite cylinder model. *Eng. Geol.* 104, 98–108. <https://doi.org/10.1016/j.enggeo.2008.09.002>.
- Selker, J.S., Thévenaz, L., Huwald, H., Mallet, A., Luxemburg, W., van de Giesen, N.,

- Stejskal, M., Zeman, J., Westhoff, M., Parlange, M.B., 2006. Distributed fiber-optic temperature sensing for hydrologic systems. *Water Resour. Res.* 42, W12202.
- Soueid Ahmed, A., Jardani, A., Revil, A., Dupont, J.P., 2013. SP2DINV: a 2D forward and inverse code for streaming potential problems. *Comput. Geosci.* UK 59-16. <https://doi.org/10.1016/j.cageo.2013.05.008>.
- Soueid Ahmed, A., Revil, A., Steck, B., Vergnault, C., Jardani, A., Vincelas, G., 2019. Self-potential signals associated with localized leaks in dam embankments and dikes. *Eng. Geol.* 253, 229–239. <https://doi.org/10.1016/j.enggeo.2019.03.019>.
- Tikhonov, A.N., Arsenin, V.Y., 1977. *Solutions of Ill-Posed Problems*. John Wiley, Washington, D.C.
- Votruba, L., Broža, V., 1989. Water management in reservoirs. In: *Developments in Water Science*. vol. 33 Elsevier Science.
- Zhdanov, M., Tolstaya, E., 2004. Minimum support nonlinear parametrization in the solution of a 3D magnetotelluric inverse problem. *Inverse Probl.* 20 (3), 937–952. <https://doi.org/10.1088/0266-5611/20/3/017/meta>.
- Zheng, C., Bennett, G.D., 2002. *Applied Contaminant Transport Modeling*, 2nd edition. A John Wiley & Sons, INC., Publication (February 2002).